07.4;09.1

Diagnostics methods of local stresses/strains in diamond at room temperature based on optically detected magnetic resonance of N*V* defects

© R.A. Babunts, A.S. Gurin, A.P. Bundakova, M.V. Muzafarova, A.N. Anisimov, P.G. Baranov

Ioffe Institute, St. Petersburg, Russia
E-mail: marina.muzafarova@mail.ioffe.ru

Received October 11, 2022
Revised October 11, 2022
Accepted November 7, 2022

A method for diagnostics of local stresses/strains in diamond at room temperature based on optically detected magnetic resonance (ODMR) of N*V* defects in a zero magnetic field using low-frequency microwave power modulation is proposed.

Keywords: N*V* defect, diamond, optically detected magnetic resonance (ODMR).

DOI: 10.21883/TPL.2023.01.55346.19391

The discovery of unique emissive properties of N*V* defects in diamond, which allow one to detect optically the magnetic resonance in the ground state of such defects (with magnetic resonance on single N*V* centers at room temperature being feasible [1,2]), opened up opportunities for ultimate miniaturization of micro- and optoelectronic components that may potentially be constructed based on a single defect. N*V* defects are used in magnetometry, thermometry, piezometry, quantum optics, biomedicine, and advanced information technology utilizing quantum properties of spins and individual photons. In order to optimize measurements, one needs to retrieve data on stress and the associated local strain in the vicinity of an N*V* defect; this should also help minimize these stress/strain values.

An individual N*V* defect (Fig. 1, *a*) is a carbon vacancy (*V*) that has one of four carbon atoms in its nearest coordination sphere substituted with a nitrogen atom. The signal of optically detected magnetic resonance (ODMR) of an N*V* center in ground state $^3A_2$ ($S = 1$) in zero magnetic field is characterized by the following standard spin Hamiltonian [2]:

$$\hat{H} = D[\hat{S}_z^2 - S(S+1)/3] + E(\hat{S}_x^2 - \hat{S}_y^2).$$

Under zero stress/strain, parameter D in diamond at room temperature assumes a value of 2870 MHz, while parameter $E = 0$ (Fig. 1, *a*). Stress in a diamond crystal or structure alters the values of D and E; while the induced relative variation of parameter D is insignificant, changes in E are absolute in nature, since they are measured from the zero E level. If the trigonal symmetry of a center is violated under strain, the degeneracy of $M_s = \pm 1$ sublevels is lifted with subsequent splitting, which depends on stress (strain) and is denoted as $\Delta = 2E$ [MHz] in Fig. 1, *a*.

ODMR of N*V* defects was used as a method for stress measurement under an external hydrostatic pressure up to 60 GPa [3] and to examine the strain coupling of an N*V* defect spin to a diamond mechanical oscillator [4] and investigate the strain-mediated coupling of the mechanical motion of a diamond cantilever to the spin of an embedded N*V* defect [5]. The variation of parameter D, which characterizes stress along the trigonal symmetry axis for an N*V* defect, and the averaged stress gradient, which is induced by the deviation of the crystal field from a trigonal one under the influence of local stress/strain, were estimated at $dD(P)/dP = 14.58$ MHz/GPa and $d(\Delta = 2E)(P)/dP \approx 35$ MHz/GPa, respectively, in these studies. The data on stress gradients from [4,5] are somewhat discrepant. In addition, all parameters were determined under external pressure and are not indicative of intrinsic stress/strain in the neighborhood of an N*V* defect. The influence of transverse strain on parameter $\Delta = 2E$ was not examined in [3].

Strain imaging in polycrystalline diamond with the use of ODMR of N*V* defects was demonstrated in [6]. The authors of [7] used the ODMR technique for in-situ measurements of fabrication-induced strain in diamond photonic structures with intrinsic N*V* centers.

The method of local stress/strain diagnostics in diamond in the vicinity of an N*V* defect at room and above-room (up to 300°C) temperatures relies on ODMR of N*V* defects in zero magnetic field. Figure 1, *b* presents the ODMR signals of N*V* defects in diamond recorded in a series of reference samples of diamonds and nanodiamonds (with different concentrations of nitrogen and N*V* defects, which were introduced into the samples in various ways). Signal *1* corresponds to a sample prepared by CVD (chemical vapor deposition), < 1 ppm N, N*V* defects were produced by nitrogen implantation with subsequent annealing; *2* — sample grown under high pressure and high temperature (HPHT), the nitrogen concentration varies within the interval of $\sim 1-100$ ppm along the diamond wafer, N*V* defects were produced by electron irradiation

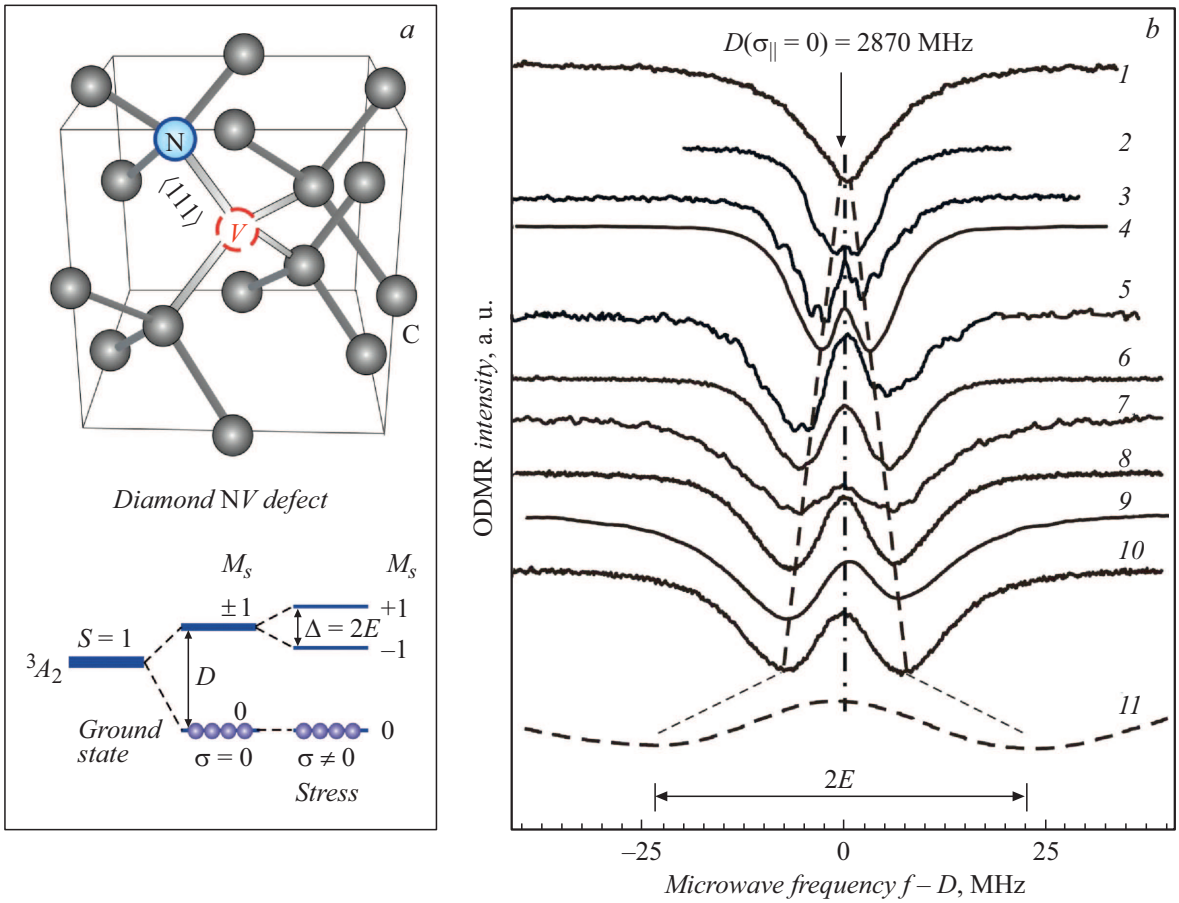

Figure 1. *a* — NV defect structure. An NV defect is in a negatively charged state (NV^-) and is characterized by electron spin $S = 1$. The fine structure of spin levels of an NV center in ground state $^3A_2$ in zero magnetic field with splitting $D = 2870$ MHz under zero stress/strain and in the presence of non-trigonal strain with a further stress/strain-dependent splitting between levels $M_s = +1$ and -1, which is denoted as $\Delta = 2E$, is shown below. *b* — ODMR signals of NV defects in diamond detected at room temperature in zero magnetic field in a series of reference samples of diamonds and nanodiamonds (with different concentrations of nitrogen and NV defects, which were introduced into the samples in various ways). See text for details.

with subsequent annealing, ODMR was detected in the crystal region with the lowest nitrogen concentration; *3* — natural type IIa diamond, < 1 ppm N, NV defects were produced by neutron irradiation with a dose of $\sim 10^{18}$ cm^{-2} with subsequent annealing; *4* — natural non-irradiated diamond; *5* — HPHT sample, ~ 200 ppm N, NV defects were produced by nitrogen implantation with subsequent annealing; *6* — HPHT sample, ~ 100 ppm N, NV defects were produced by neutron irradiation with subsequent annealing; *7* — polycrystalline nanodiamond (non-irradiated, non-annealed); *8* — Element-6, HPHT, ~ 100 ppm N, NV defects were produced by proton irradiation with subsequent annealing; *9* — commercial nanocrystal (300 nm), 100–120 ppm N, 3 ppm NV; *10* — non-irradiated nanodiamonds sintered under HPHT conditions, high concentration of NV defects (~ 50 ppm) and a substitutional nitrogen concentration (based on EPR data) up to 500 ppm (see [8] for details) were measured; *11* — detonation-synthesized nanodiamond 5 nm in diameter with individual NV defects (data from [9]).

The variation of splitting $\Delta = 2E$ of the central ODMR line in different samples, which is induced by local stress/strain in the vicinity of an NV defect, is evident. We introduce two limit values of internal local stress/strain in a diamond crystal.

1. Spin Hamiltonian parameter $E = 0$ for an ideal unstressed structure is taken as the zero reference point.

2. The splitting between levels $M_s = -1$ and $+1$, which is equal to $\Delta = 2E = 46$ MHz in detonation-synthesized nanodiamond ~ 5 nm in diameter and is, as far as we know, the maximum splitting recorded for internal local stress/strain in diamond at the position of an NV defect, is taken as the maximum point. This splitting was measured in [9].

It can be seen from Fig. 1, *b* that all splitting magnitudes $\Delta = 2E$ fall within the interval between the indicated two limit values: 0 and 46 MHz. Stress σ [MPa] and relative strain ε, which is proportional to σ, are determined based on the values of $\Delta = 2E$ for each reference sample in

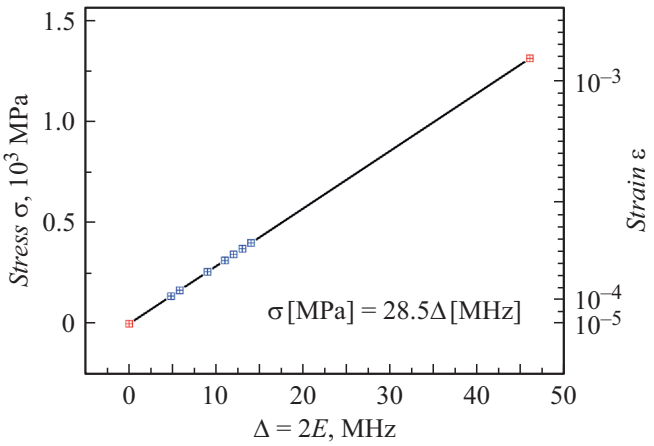

Figure 2. Calibration curve for the dependence of stress σ and relative strain ε on the magnitude of splitting $\Delta = 2E$ between levels $M_s = +1$ and -1. The straight line corresponds to formula σ [MPa]=28.5Δ [MHz] that characterizes this dependence and allows one to determine stress/strain at the position of an NV center.

accordance with the following formula: $E_{diam} = \sigma/\varepsilon$, where the Young's modulus for diamond is $E_{diam} = 1200$ GPa.

The calibration curve for the dependence of stress σ and relative strain ε on $\Delta = 2E$ is shown in Fig. 2. Figure 3 presents ODMR signals (*1* and *2*) in two regions, which are highlighted by focused laser radiation, within high-pressure high-temperature diamond irradiated by electrons with subsequent annealing that has a nitrogen concentration varying in the $\sim 10-100$ ppm interval along the wafer. The concentration of N and NV defects is shown in arbitrary scale in shades of gray. Curve *3* is presented for comparison and corresponds to the ODMR signal in natural diamond with the hyperfine structure (HFS) for ^{14}N, which is contained in an NV defect, manifesting itself in the form of three lines with a splitting of ~ 2 MHz that serve as a natural scale. HFS with the same ~ 2 MHz splitting, which is independent of $\Delta = 2E$, is also seen in the ODMR spectrum of NV defects localized at the point of the lowest nitrogen concentration (spectrum *1*). The corresponding splitting $\Delta = 2E$ also assumes its minimum value. The photoluminescence (and, consequently, ODMR signal) intensity is approximately 500 times lower than the signal intensity in the darkest part of the sample (spectrum *2* in Fig. 3) with the maximum nitrogen concentration.

One needs to decompose the ODMR spectrum into two lines with splitting $\Delta = 2E$ in order to determine E more accurately. The results of this decomposition are represented by dashed curves. We thus obtain a value of 5.4 MHz for the distance between maxima in the experimental spectrum, while the result of decomposition is 6.3 MHz; i.e., the splitting is $\Delta = 2E = 5.85 \pm 0.45$ MHz on average. The terrestrial magnetic field induces ODMR line broadening, which does not exceed 1 MHz in magnitude. This does not have any significant effect on measurement results, since HFS splitting due to the interaction with nitrogen ^{14}N within an NV center also broadens the ODMR line. However, the external magnetic field in precision measurements of small (< 1 MHz) $\Delta = 2E$ splitting values should be compensated with Helmholtz coils. This allows one to narrow ODMR lines down and determine splitting $\Delta = 2E$ more accurately (see Fig. 3).

A calibration curve for the dependence of D on external pressure was obtained in [3]; at the same time, data on the influence of external stress/strain on parameter E (i.e., stress/strain in the direction perpendicular to the trigonal axis of an NV defect) were not provided. The same can be said about [5]. However, the authors of [3] presented ODMR spectra, wherein ODMR line splitting due to the presence of an uncontrolled perpendicular stress/strain component was observed under high hydrostatic pressures. Specifically, splitting $\Delta = 2E = 26$ MHz between spin levels $M_s = -1$ and $+1$ was measured under a hydrostatic pressure of 60.4 GPa. In accordance with the calibration curve in Fig. 2, this splitting corresponds to stress $\sigma = 740$ MPa and relative strain $\varepsilon = 6.17 \cdot 10^{-4}$.

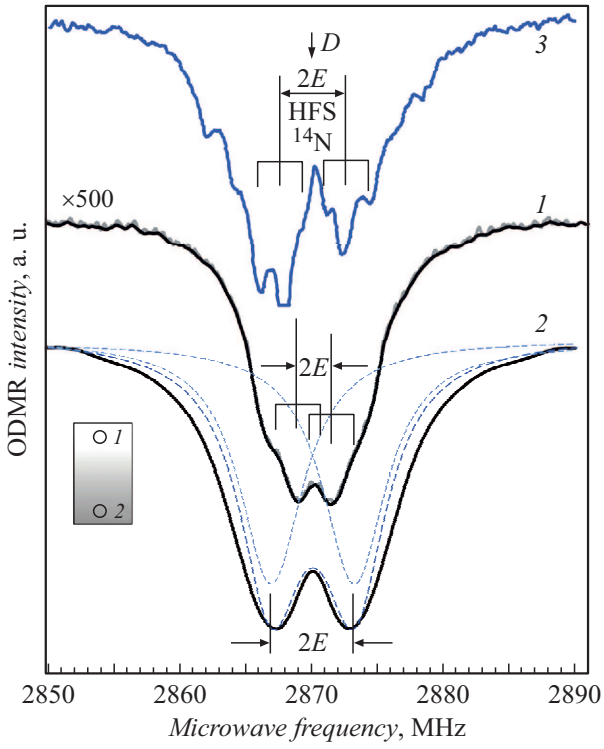

Figure 3. ODMR signals in two diamond crystal regions, which are highlighted by focused laser radiation, with a nitrogen concentration varying along the diamond wafer (*1*, *2*). The concentration of nitrogen and NV defects for these two regions is shown in arbitrary scale in shades of gray. Curve *3* is presented for comparison and corresponds to the ODMR signal in natural diamond (spectrum *4* in Fig. 1, *b*) with the hyperfine structure (HFS) for nitrogen ^{14}N, which is contained in an NV defect, manifesting itself in the form of three lines with a splitting of ~ 2 MHz that serve as a natural scale.

We note in conclusion that splitting $D = 2880\,\text{MHz}$ was measured in [9]; i.e., the shift relative to an NV defect in unstressed diamond is $+10\,\text{MHz}$, and a local compressive stress of 685 MPa is present. We may also assume that the sign of E is positive (i.e., local compression in the transverse plane is in effect). Thus, the obtained value of $\Delta = 2E = 46\,\text{MHz}$ corresponds to compressive stress $\sigma = 1310\,\text{MPa}$ and relative compressive strain $\varepsilon = 1.09 \cdot 10^{-3}$.

Funding

This study was supported by a grant from the Russian Science Foundation (project No. 20-12-00216).

Conflict of interest

The authors declare that they have no conflict of interest.

References

[1] A. Gruber, A. Drabenstedt, C. Tietz, L. Fleury, J. Wrachtrup, C. Von Borczyskowski, Science, **276**, 2012 (1997). DOI: 10.1126/science.276.5321.2012
[2] P.G. Baranov, H.-J. von Bardeleben, F. Jelezko, J. Wrachtrup, *Magnetic resonance of semiconductors and their nanostructures: basic and advanced applications*. Springer Ser. in Materials Science (Springer-Verlag, Vienna, 2017), vol. 253.
[3] M.W. Doherty, V.V. Struzhkin, D.A. Simpson, L.P. McGuinness, Y. Meng, A. Stacey, T.J. Karle, R.J. Hemley, N.B. Manson, L.C.L. Hollenberg, S. Prawer, Phys. Rev. Lett., **112**, 047601 (2014). DOI: 10.1103/PhysRevLett.112.047601
[4] J. Teissier, A. Barfuss, P. Appel, E. Neu, P. Maletinsky, Phys. Rev. Lett., **113**, 020503 (2014). DOI: 10.1103/PhysRevLett.113.020503
[5] P. Ovartchaiyapong, K.W. Lee, B.A. Myers, A.C. Bleszynski Jayich, Nature Commun., **5**, 4429 (2014). DOI: 10.1038/ncomms5429
[6] M.E. Trusheim, D. Englund, New J. Phys., **18**, 123023 (2016). DOI: 10.1088/1367-2630/aa5040
[7] S. Knauer, J.P. Hadden, J.G. Rarity, npj Quantum Information, **6**, 50 (2020). DOI: 10.1038/s41534-020-0277-1
[8] P.G. Baranov, A.Ya. Vul', S.V. Kidalov, A.A. Soltamova, F.M. Shakhov, *Sposob polucheniya almaznoi struktury s azotno-vakansionnymi defektami*, RF Patent 2448900 (priority date July 28, 2010; registered at the State Registry of Russia on April 27, 2012) (in Russian).
[9] C. Bradac, T. Gaebel, N. Naidoo, M.J. Sellars, J. Twamley, L.J. Brown, A.S. Barnard, T. Plakhotnik, A.V. Zvyagin, J.R. Rabeau, Nature Nanotechnol., **5**, 345 (2010). https://www.nature.com/articles/nnano.2010.56